15th International Plansee Seminar, Eds. G. Kneringer, P. Rödhammer and H. Wildner, Plansee Holding AG, Reutte (2001), Vol. 4

The Manufacture of Carbon Armoured Plasma-Facing Components for Fusion Devices

B.Schedler, Th.Huber, A.Zabernig, F.Rainer, K.H.Scheiber, D.Schedle

Plansee AG, A-6600 Reutte, Austria

Summary:

Within the last decade Plansee has been active in the development and manufacture of different Plasma-Facing-Components for nuclear fusion experiments consisting in a tungsten or CFC-armour joined onto metallic substrates like TZM, stainless steel or copper-alloys. The manufacture of these components requires unique joining technologies in order to obtain reliable thermo mechanical stable joints able to withstand highest heat fluxes without any deterioration of the joint. In an overview the different techniques will be presented by some examples of components already manufactured and successfully tested under high heat flux conditions. Furthermore an overview will be given on the manufacture of different high heat flux components for TORE SUPRA, Wendelstein 7-X and ITER.

Keywords:

Joining, C/C, CuCrZr, TZM, Active Metal Casting, Laser treatment, Brazing, ITER, Tore Supra, Wendelstein 7-X, RFX, Divertor, High Heat Flux Components, NDT, radiographic examination, ultrasonic examination, thermography

Introduction:

In the last decade an extensive technology development program has been carried out by Plansee on the manufacture of carbon armoured high heat flux components for nuclear fusion experimental reactors. Beside the development and manufacture of prototypes for the german stellerator experiment Wendelstein 7-X and ITER[1], which is a triplate, collaborative project carried out by the European Union, Japan and the Russian Federation, Plansee has also supplied the thermally highest loaded components for the French Tokamak experiment Tore Supra, namely a part

15th International Plansee Seminar, Eds. G. Kneringer, P. Rödhammer and H. Wildner, Plansee Holding AG, Reutte (2001), Vol. 4

of the Inner First Wall, Antennae Limiter and Toroidal Pumped Limiter. All these components consist in at least one portion of C/C composite that has to be joined onto metals like molybdenum, stainless steel or copper alloys. The main obstacle to overcome is the realisation of a reliable joint dealing with heat fluxes up to 30MW/m² and the associated thermo mechanical loads.
The approach of Plansee comprising elements like laser structuring[2] of the joint area or Active Metal Casting[3] has proven its reliability under to above described thermal load and is regarded as the reference solution for ITER [1].

Design of Relevant Components

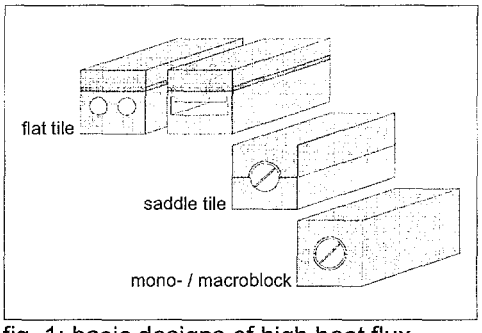

fig. 1: basic designs of high heat flux components for divertors

In the frame of the ITER EDA[4] several plasma facing component designs have been proposed [2]. Each of them has specific advantages and extensive testing has shown that they could sustain the requirements. The three main options depend on the bonding of the plasma facing material to the heat sink. A sketch of each is shown in fig. 1. The flat tile design is the most common and easiest to manufacture. The joining interface is flat and allows an easy fitting with rectangular heat sinks having different types of cooling concepts. Straight tubes with or without turbulance promoters (fins, swirl tapes etc.) are the simplest cooling structures with reasonable performance. Hypervapotrons are more sophisticated options revealing improved performance. In the flat tile geometry a stress singularity occurs at the free edge of the interface. The strength of this singularity depends on the elastic properties and on the coefficient of thermal expansion of the dissimilar materials, on the shape of the interface and on the temperature field.
The saddle block consists of a series of separate heat sink square blocks connected by a concentric tube and protected by a saddle shaped armour. It is an improvement of the proceeding one with the bonding interface closer to the coolant fluid.

[2] patent: EP 0 476 772 B1
[3] patent: EP 0663 670 B1
[4] EDA...Engineering Design Activities

15th International Plansee Seminar, Eds. G. Kneringer, P. Rödhammer and H. Wildner, Plansee Holding AG, Reutte (2001), Vol. 4

The monoblock, consisting of a series of individual armour square blocks connected by a concentric tube, removes the stress singularity by eliminating the flat interface. The monoblock or macroblock design takes the advantage of the carbon composites thermomechanical properties. The bonding interface is the circular cooling tube which gives the lowest possible temperature for the joint. The high thermal conductivity, the low elastic modulus and the low thermal expansion coefficient reduce drastically the thermomechanical stresses of this concept. This design allows for large massive blocks, having structural properties, which reduce local peaking heat fluxes by spreading out the heat flow through the carbon monoblock. By now the components based on the monoblock design outperformed by far the flat tile and saddle designs.

Manufacturing Route according to the Plansee Approach

Reliable metal-C/C composites require beside a perfect wetting of the braze alloy also the mastering of stresses generated due to the mismatch of properties of the different materials to be joined. In the manufacturing approach applied by Plansee both issues are considered, combining a LASER treatment of the C/C joint surface with the so called active metal casting process. The reliability and outstanding performance of components manufactured with these two techniques have been demonstrated within the devolpment activities of carbon armoured plasma facing components for nuclear fusion experiments [1,3,8,9,10,11, 12].

Laser Structuring

An important consideration in making dissimilar materials joints relates to the thermal mismatch stresses and strains. In any joining of portions of two dissimilar materials the mismatch in CTE is extremely important. From the mismatch of their thermal expansion thermal stresses result. The magnitude of these mismatch stresses and strains determines the failure probability of the joint. These mismatch stresses and strains must be carefully controlled. According to Hagy and Ritland [5] the CTE mismatch differentials of within 100ppm are considered as allowable for reliable dissimilar material joints. An important problem with common joining processes is the understanding and control over a period of cooling time the mismatches in CTE and thermal strain and stress gradients in the joint region.
At Plansee these considerations have led to the development of a microengineered joint interface. With this process a LASER drills conical

15th International Plansee Seminar, Eds. G. Kneringer, P. Rödhammer and H. Wildner, Plansee Holding AG, Reutte (2001), Vol. 4

holes into the joining interface C/C part. A typical metallographic cut of a brazed sample with such a structured interface shall be demonstrated in fig. 2. Depending on the metallic substrate such laser treated Graphite or C/C parts can be joined directely by usual brazing processes onto metallic substrates like molybdenum, stainless steel or copper.

The outstanding positive influence of such a treatment can be easily demonstrated by thermal shock experiments. Under standardized quenching conditions there is a one-to-one correspondence between the joint strength and the allowable initial quenching temperature [6]. This temperature can be regarded as a direct measure of the joint strength for a specific joint configuration.

In order to test the integrity of the joint such quench tests have been performed in the frame of the qualification procedure for the inner first wall of Tore Supra [3]. Metal-C/C composites samples have been prepared representing the joint being used for the inner first wall of Tore Supra. These samples consisted of a C/C joined onto stainless steel via an intermediate 2mm thick OFHC-copper layer joined with a Ti-Cu-Ag braze alloy. One part of the samples has been joined without laser treatment whereas the other part of the samples revealed a LASER treated surface. Samples with microengineered surfaces survived 20 thermal shock cycles from 600°C to cold water without destruction whereas samples without laser treatment have been damaged after a few cycles. During later exposure to the plasma the components manufactured with this qualified technology could sustain heat fluxes up to 1 MW/m² without any deterioration [12] during a several years lasting operation period. The positive influence of the structuring might be explained by different effects. By such a structure a graded-material is created in the joint region smoothening the transition of properties. Finite Element Calculations [4] further revealed that the stress in the structured CFC portion is reduced by a transfer of the load from the CFC into the metallic portion cast into the cones. Furthermore also the propagation of cracks in the brittle carbide interface is impeded.

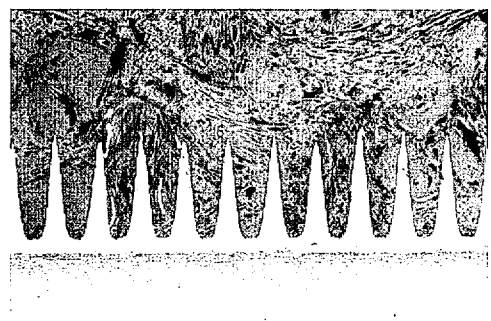

fig. 2: laser structure brazing interface (C/C joined onto TZM with TiCuAg

15th International Plansee Seminar, Eds. G. Kneringer, P. Rödhammer and H. Wildner, Plansee Holding AG, Reutte (2001), Vol. 4

Active Metal Casting

In general the joining of metals to graphite or ceramic materials is not only a problem due to the residual stresses caused by the mismatch of properties, but also due to metallurgical reasons. Usually active Brazing is the prime choice in order to obtain metal-C/C joints. Carbide forming elements out of the group IV and V are constituents of such active braze alloys. These elements react with the C/C joint surface and make it wettable for the liquid metals of the braze alloy. However, due to the materials involved such brazed components often suffer from difficult to control processes resulting in braze flaws. The probability of braze flaws increases with increasing joint area, leading to the rejection of the whole component. In order to overcome this critical issue Plansee has developed the Active Metal Casting process.
With this process a non-carbide forming metal like copper is cast onto the C/C composite in the presence of Titanium. During this process the Titanium reacts with the C/C composite by the formation of a TiC interlayer, which then can be wet be the liquid copper. This process can be applied to a wide range of geometries such as straight and bent flat tiles and monoblocks (fig. 3). Usually this process in combined with the above described LASER structured interface in order to deal with the stress occurring during the cooling from the casting temperature (fig. 4).

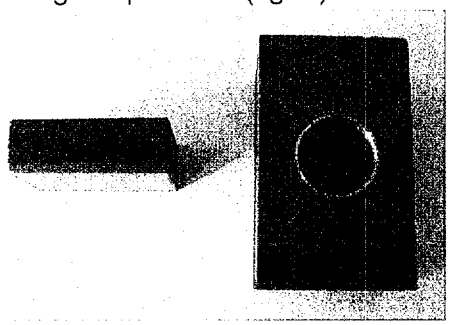

fig. 3 active metal cast C/C flat tile and monoblock

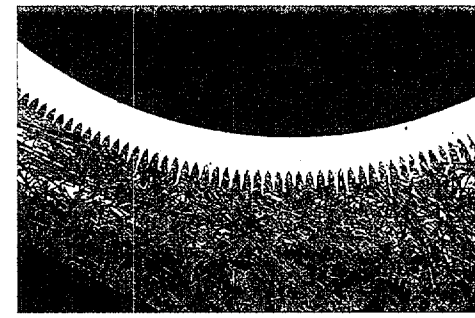

fig. 4: active metal cast interface with laser structured C/C

With such laser treated, active metal cast C/C flat tiles or monoblocks a copper layer is generated on the graphitc substrate, which then acts as metallic interface for further less critical and more reliable metal/metal joints by applying techniques like brazing, Electron Beam Welding, Hot Isostatic Pressing or Diffusion Bonding for the joining of the C/C armour onto the heat sink. This possibility opened by the Active Metal Casting Process is interesting for Heat Flux Components consisting of materials sensitive to heat treatments like age-hardening Cu-alloys.

15th International Plansee Seminar, Eds. G. Kneringer, P. Rödhammer and H. Wildner, Plansee Holding AG, Reutte (2001), Vol. 4

Compared to a direct brazing operation of the CFC onto a metallic heat sink the intermediate active metal casting step allows a 100% non destructive inspection of the critical metal-C/C joint prior to final joining onto the heat sink. At Plansee this non-destructive inspection is usually done by radiography, judging the wetting and penetration of the cast metal into the C/C composite. Such a pre-selection of the critical metal to C/C joints is a big advantage with regard to large components, where even one bad metal-C/C joint results in the rejection of the whole component.

Manufacture of Antennae and Toroidal Pumped Limiter for TORE Supra

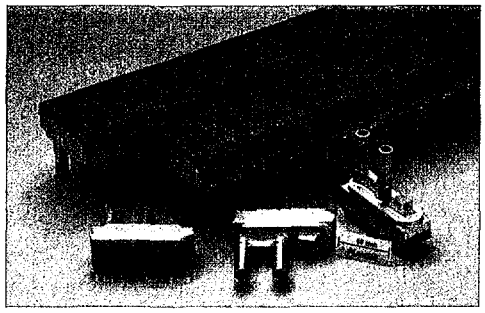

fig. 5: Antennae Limiters

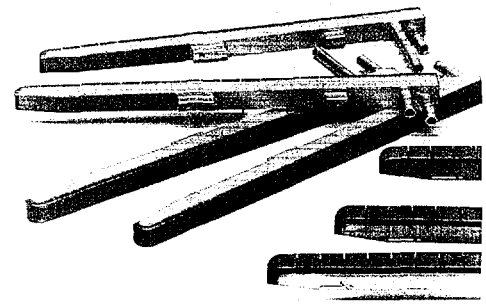

fig. 6: Toroidal Pumped Limiter

For the French nuclear fusion experiment TORE SUPRA Plansee manufactured beside a part of the inner first wall also 250 Antennae Protection Limiters and the 600 Toroidal Pump Limiter (see fig. 5 and 6). Both types of components consist in laser structured, active metal cast C/C flat tiles joined onto a CuCrZr heat sink by means of deep penetration electron beam welding [7]. As it can be seen on the images it is possible to apply the described techniques not only to flat but also to bent C/C tiles. The quality of the active metal cast interface is judged by means of radiographic inspection whereas the electron beam weld is judged by ultrasonic inspection. Flaws with maximum Ø3mm are accepted for both cases. After successfully passing these non destructive examination the cooling channels are machined into the CuCrZr armour. Subsequently the cooling system is closed by plugs joined by electron beam welding. For the transition of the copper cooling system to the stainless steel cooling system of the TORE SUPRA machine an electron beam welded dog-bone joint geometry comprising an intermediate Ni-layer has been applied. For final acceptance the components undergo a series of non-destructive examinations like a hot-helium leak test operating at 250°C/40 bar internal He-pressure, followed by a transient thermographic

15th International Plansee Seminar, Eds. G. Kneringer, P. Rödhammer and H. Wildner, Plansee Holding AG, Reutte (2001), Vol. 4

inspection carried out by flooding the cooling system with hot steam (250°C/40 bar) and measuring the thermal response of the C/C surface. Fig. 7 shall summarize all the destructive and non-destructive inspection steps necessary within the manufacture of these critical components.

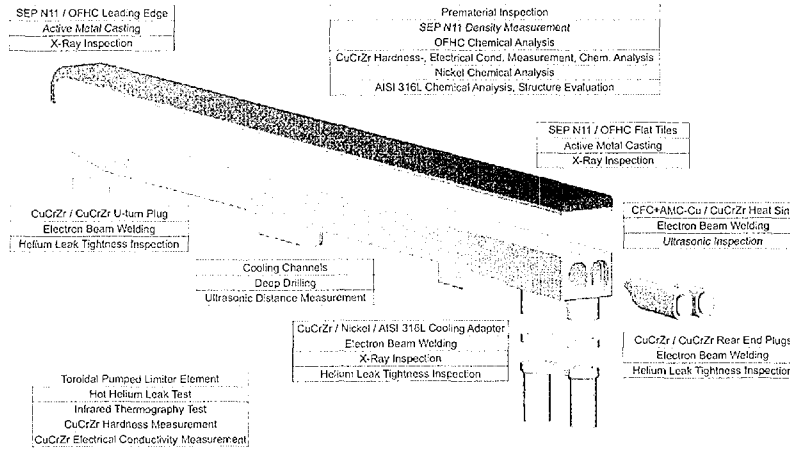

fig. 7: Manufacture and Test Sequence of Toroidal Pumped Limiters

Manufacture of prototypical High Heat Flux Components for ITER with C/C monoblock armour joined onto CuCrZr-tubes

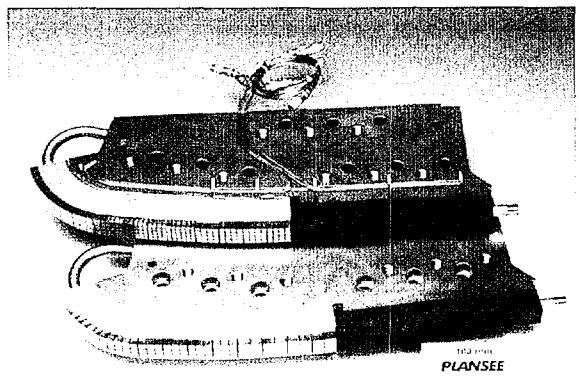

fig. 8 ITER Vertical Target Medium Scale Mock-Up

For areas like the divertor for ITER the C/C armoured components are envisaged as the reference solution [8]. In the lower area of these components heat loads up to 20MW/m² are expected during so-called "slow transients" As described above monoblocks proved to be the most robust solution to cope with these extremely demanding operating conditions.

15th International Plansee Seminar, Eds. G. Kneringer, P. Rödhammer and H. Wildner, Plansee Holding AG, Reutte (2001), Vol. 4

The first generation of C/C monoblock components was developed in the mid 90th. The reference manufacturing technology has been active metal casting of a 0,5 – 1,0mm thick OFHC copper interlayer onto the laser structured surface of a drilled bore of a CFC tile [9]. The AMC C/C monoblock is then joined onto the copper alloy tube (PH-Cu alloy CuCrZr or DS-Cu alloy GlidCop®) by an eutectic Ti-Cu brazing at 880°C. Following this manufacturing route a medium scale vertical target prototype has been manufactured and tested (fig. 8). This component contained all the main features of the ITER divertor design and had an overall length of about 600mm. The high heat flux part had a lower straight section made of C/C monoblocks and an upper bent region with a tungsten macrobrush flat tile armour. The heat sink has been manufactured from the DS-Cu alloy GlidCop® by HIP of a bent GlidCop® tube into two GlidCop® half shells. Onto this heat sink the tungsten macrobrush flat tiles comprising a cast OFHC layer have been joined by electron beam welding. The AMC C/C monoblocks have then been joined onto the GlidCop®-tube by an eutectic Ti-Cu brazing at 880°C. A twisted tape with a twist ratio of 2 was inserted in the monoblock region to enhance the critical heat flux limit. This component has then been tested at FE200 electron beam facility at FRAMATOME in Le Creusot, France on both the tungsten and the C/C armour at 10MW/m² without any failure. The C/C monoblocks has further been tested up to 30 MW/m² without any failure.

The results of the R&D activities carried out on copper alloys revealed that DS-Cu has a very poor fracture toughness which together with low creep resistivity and weldability has triggered the choice of the reference heat sink material to the precipitation hardened material CuCrZr. Furthermore components with a bent C/C monoblock section are required. These considerations led to the need for developing a new manufacturing technology because the brazing technique at 880°C was not compatible with the use of CuCrZr as heat sink material.
An extensive R&D has been carried out by Plansee to develop an optimised manufacturing process for active metal cast CFC monoblocks fully compatible with the use of CuCrZr alloy. The selected manufacturing process was Hot Isostatic Pressing of OFHC copper active metal cast C/C monoblocks onto solution annealed water quenched CuCrZr tubes, which are age hardened during the HIP cycle. With this process it has been possible for the first time to manufacture bent C/C monoblock components as it is shown in fig. 9 and 10.

15th International Plansee Seminar, Eds. G. Kneringer, P. Rödhammer and H. Wildner, Plansee Holding AG, Reutte (2001), Vol. 4

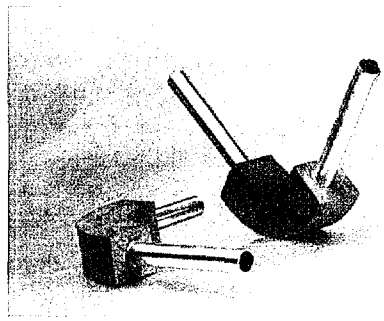

fig.9: Curved C/C monoblock mock-up

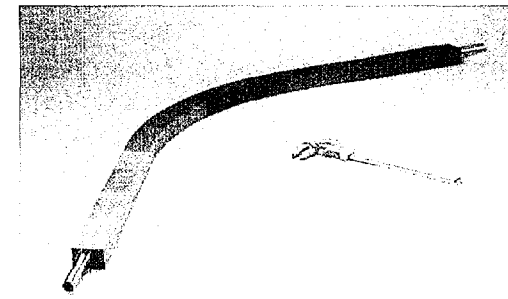

fig. 10:ITER Divertor Full Scale Prototype

The components of fig. 9 represent small scale mock-ups manufactured by HIP in the frame of the qualification of this technology. These mock-ups have been successfully tested under high heat flux with electron beam up to 18MW/m². Based on this technology a full scale ITER Divertor high heat flux component (length 1200mm) shown in fig. 10 has been manufactured. This component consists in a section of tungsten and a CFC monoblocks, respectively. Both monoblock types comprise a OFHC copper interlayer in the bore hole, which has been used for the joining onto the CuCrZr tube by Hot Isostatic Pressing.

Manufacture of prototypical High Heat Flux Components for Wendelstein 7-X

The open divertor design proposed for the stellerator experiment Wendelstein 7-X, currently under construction at Greifswald (D), consists of 10 independend divertor units with an overall target plate area of 22m², formed of approximately 1500 actively cooled elements [10,11]. The target plates are designed for steady state operation with a local heat load of up to 10MW/m². Because of the geometrical boundary conditions in the W7-X vessel, the target plates have to be very thin, which is why a flat tile design with C/C flat tiles brazed onto a TZM water cooled heat sink was selected. The thickness of the C/C tiles was restricted with 6mm in order to keep a surface temperature limit of maximum 1200°C for the highest power load. In order to increase the thermal transfer coefficient between the heat sink and the cooling water a fin design with 5 fins per cooling channel has been chosen. In fig. 11 a target element cross section is shown. It consists of the laser structured C/C flat tiles, the TZM fin plate heat sink and the TZM back plate with for parallel cooling channels.

15th International Plansee Seminar, Eds. G. Kneringer, P. Rödhammer and H. Wildner, Plansee Holding AG, Reutte (2001), Vol. 4

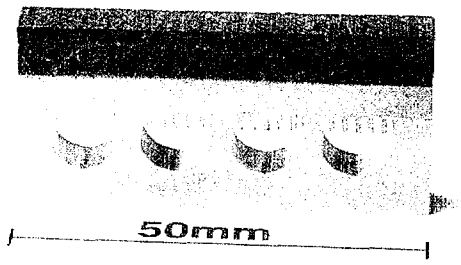

fig.11: Cross section of W7-X prototypical divertor target plates

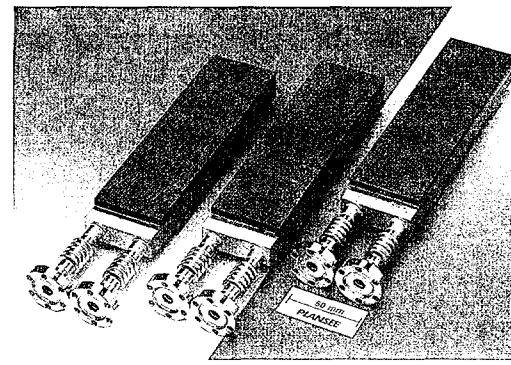

fig.12: Prototypical W7-X divertor target plates C/C joined onto TZM

The manufacturing route of the target elements was determined by the requirement of a complete 100% non-destructive inspection of all braze interfaces. This led to a specific feature of the manufacturing route, i.e. the split of the brazing operation in two cycles. The first between the laser structured C/C tiles and the TZM-fin plates (TiCuSil / 850°C), the second between the TZM fin plate and the TZM back plate (AgCuPd / 810°C). For such a sequence high precesion is demanded in order to compensate for the warpage induced by the different thermal expansion coefficients of the C/C composite and the TZM.

Such a way manufactured elements have then been tested using the electron beam device JUDITH of the KFA Jülich with a stationary power load up to 12MW/m² without any detachment of the C/C tiles.

15th International Plansee Seminar, Eds. G. Kneringer, P. Rödhammer and H. Wildner, Plansee Holding AG, Reutte (2001), Vol. 4

References:

[1] International Thermonuclear Experimental Reactor, Technical Basis for the ITER Final Design Report, Cost Review and Safety Analysis, IAEA, Vienna 1998, Chapter II-Section 4.1 – Page 34

[2] Ph.Chappuis et al., Possible Divertor Solutions for a Fusion Reactor. Part 2. Technical Aspects of a Possible Divertor,
Fusion Engineering and Design, Volume 36/1 (1997), page 109-117

[3] M.Lipa et al., Development and fabrication of improved CFC-brazed components for the inner first wall of Tore Supra, Proceedings of the 19th Symposium on Fusion Technolgy, Lisbon, Portugal, 16-20 September 1996

[4] Plansee Internal Report

[5] Hagy and Ritland, Viscosity Flow in Glass-to-Metal Seals, J. Amer.Ceram.Soc., Vol. 40, pp 58-62, 1957

[6] Chou H.Li, Ceramic Composite, United States Patent, 5.874,175,

[7] Kneringer et al., EP 0 741 116 B1, Process for Manufacturing of components with high thermal load capability

[8] International Thermonuclear Experimental Reactor, Technical Basis for the ITER final design report, cost review and safety analysis (FDR), chapter II-section 4.1-page 33, IAEA, Vienna 1998

[9] G.Vieider et al., European development of the ITER Divertor target, Fusion Eng. Des. 46, 221 (1999)

[10] Renner H. et al., J.Nucl.Mater., 241-243, 946-949, (1997)

[11] Greuner H. et al., Design, Manufacture and Testing of the W7-X Target Element Prototypes, Proceedings of the 19th Symposium on Fusion Technology, Fusion Technology, Vol. 1, 463-466 (1996)

[12] Schlosser J. et al., Experience Feedback from High Heat Flux Component Manufacturing for Tore Supra, Proceedings of the 21th SOFT conference, 11.-15. September 2000 Madrid, Spain, in press

15th International Plansee Seminar, Eds. G. Kneringer, P. Rödhammer and H. Wildner, Plansee Holding AG, Reutte (2001), Vol. 4

PROCESSING OF NANO SIZED TITANIUM NITRIDE REINFORCED TITANIUM COMPOSITES

V.V. Dabhade, M.M. Godkhindi*, T.R. Rama Mohan, P. Ramakrishnan and E. Y. Gutmanas.**

Department of Metallurgical Engineering and Materials Science
Indian Institute of Technology, Bombay, Mumbai, India.

*Department of Metallurgical and Materials Engineering
Indian Institute of Technology, Kharagpur, India.

** Israel Institute of Technology, Haifa, Israel.

SUMMARY:

Attempts have been made to study the effect of nano sized TiN reinforcement loading, sintering temperature and atmosphere on the densification behavior of titanium - titanium nitride nanocomposites. Titanium with average particle size of 2 microns and titanium nitride with a particle size of the order of 50 nanometers were used in the present investigation. The compacts showed good sinterability both in argon and nitrogen atmospheres. The initial stage of sintering of pure Ti as well as Ti-TiN nanocomposites has been studied by using the constant rate of heating technique. The frequency factor (D_o), activation energy for sintering (Q) and diffusion coefficient (D) have been evaluated and discussed for the Ti and Ti-TiN nanocomposites sintered in argon and nitrogen atmospheres. Sintering of Ti and Ti-TiN nanaocomposites in nitrogen atmosphere is affected by two competing mechanisms such as endothermic activation energy required for mass transport mechanism and an exothermic energy due to insitu nitridation reaction. Microstructural studies have been carried out to supplement the densification data.

KEYWORDS:

Titanium, Titanium Nitride, Nanocomposite, Sintering, Frequency factor, Activation energy, Diffusion coefficient.

15th International Plansee Seminar, Eds. G. Kneringer, P. Rödhammer and H. Wildner, Plansee Holding AG, Reutte (2001), Vol. 4

1. INTRODUCTION:

Titanium is the design choice for many aerospace, automotive, medical, marine, chemical processing and biomedical applications because it offers low density, outstanding corrosion resistance and good mechanical properties at room and moderately elevated temperatures [1-3]. Despite the fact that titanium is the best choice for many systems from the stand point of performance durability, less titanium is used in the final production because of the high cost of the components which includes the initial cost of metal, the cost of processing and forging and the cost of machining. As a result, net shape or near-net shape technologies are one of the major avenues for reducing the cost of titanium components. These processes include isothermal forging, casting, superplastic forming and powder metallurgy [3]. Titanium powder metallurgy offers the potential for true net shape capability, an efficient material utilization combined with mechanical properties that are equal to or exceed cast and wrought products [4,3]. It also allows a four to five fold increase in metal utilization and a one to two fold decrease in labor consumption [5].

Titanium matrix composites (TMC's) are processed by the incorporation of high modulus and high strength reinforcements into titanium. Titanium itself possesses a high specific strength at room and moderately elevated temperature and due to the incorporation of these reinforcements there is a significant improvement in its specific modulus, specific strength and creep resistance [6]. Titanium nitride (TiN) is an important reinforcement candidate material for TMC's. Titanium nitride possesses unique properties like high hardness, stability at high temperatures, and electrical and optical properties that are highly desirable for a variety of applications. Titanium nitride is used for cutting tools, tool coatings, solar-control films, and microelectronics applications. It is harder than alumina, thermally stable to about 3300K, chemically stable with respect to most etching solutions and provides an excellent diffusion barrier against metals [7].

Particulate reinforced TMC's have been mainly processed by solidification/casting process and powder metallurgy. The high melting point of titanium (1933 K) and its high reactivity in the liquid state are the major limitations in processing particulate TMC's by the solidification/casting process [6]. Powder metallurgy provides an excellent route for the processing

15th International Plansee Seminar, Eds. G. Kneringer, P. Rödhammer and H. Wildner, Plansee Holding AG, Reutte (2001), Vol. 4

of particulate TMC's provided homogeneous distribution of the reinforcing phase takes place [8].

A nano-composite is a composite consisting of two or more phases where atleast one of the phases is in the nano range (< 100 nm). Because of the extremely small dimensions of the particles a large volume fraction of the atoms are located at the grain boundaries, and this confers special attributes to these materials. The properties of titanium nano-composites are very often superior to those of conventional coarse-grained TMC's. Titanium nano-composites exhibit higher strength/hardness, enhanced diffusivity, improved ductility/toughness when compared with conventional coarse-grained TMC's [9]. Several novel processing methods have been developed to synthesis nanosized powders from which nano-composites are processed. These processes can be classified broadly as mechanical synthesis [2,10], thermochemical synthesis [11] and chemical synthesis [12]. Titanium nano-composites can be synthesized from these powders by consolidation techniques like pressureless sintering, sinter-forging, hot pressing and hot isostatic pressing [13].

In the present investigation, attempts have been made to study the effect of nano sized TiN reinforcement loading, sintering temperature and atmosphere on the densification behavior of Ti-TiN nano-composites, processed by the powder metallurgy route.

2. EXPERIMENTAL:

Elemental titanium powder (99.8% purity) of average particle size of 2 μm and nano sized titanium nitride powder of average particle size of 50 nm were used in the present investigation. The particle size was measured using TEM. Three sets of powders were prepared. First set of elemental titanium, second set of powder mixture of elemental titanium with 8-wt % of titanium nitride and third set of powder mixture of elemental titanium with 15-wt % of titanium nitride. The powder mixtures were prepared by manual mixing in a mortar and pestle followed by ultrasonic mixing, while the same treatment was also given to the set of elemental titanium powder. The powder sets were then compacted uniaxially in a rigid die of 12 mm diameter at a pressure of 435 MPa. The compacts were then sintered in a rapid heating tubular furnace at five different temperatures in the range of 900-1100°C for 30 min. Sintering experiments were repeated in two different sintering atmospheres of argon and nitrogen.

15th International Plansee Seminar, Eds. G. Kneringer, P. Rödhammer and H. Wildner, Plansee Holding AG, Reutte (2001), Vol. 4

3. RESULTS AND DISCUSSION:

3.1 Characterization of Powders

Figures 1(a) and 1(b) show the TEM photographs of pure titanium and titanium nitride powders respectively. The reported values of the particle size of titanium and titanium nitride powders measured by TEM are the average of at least 25 readings. The powders were also subjected to X-ray diffraction (XRD) analysis and they revealed that titanium was in α form and both titanium and titanium nitride were single-phase structures (no peaks corresponding to any other Ti_xN phase were observed). TEM photographs of the starting powders clearly reveal that Ti powder is micron-sized and TiN powder is of nanometric size though both the powders do show a tendency to form clusters and agglomerates.

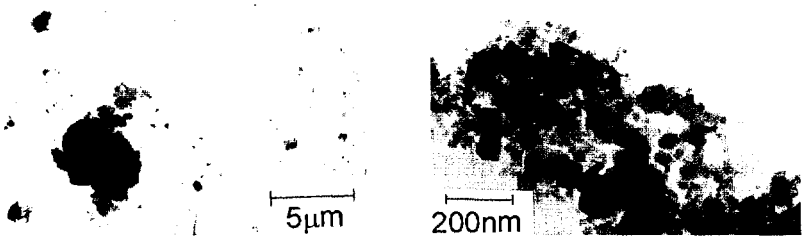

Figure 1: TEM photographs of (a) pure Ti powder and (b) TiN powder.

3.2 Sintering of elemental titanium compacts

Figure 2(a) indicates the variation of sintered density as a function of sintering temperature for pure titanium samples sintered in argon and nitrogen atmospheres. It can be seen that the sintered density increases in both the atmospheres. Within the narrow temperature range studied, the sintered densities seem to increase linearly as a function of sintering temperature. The rate of sintering seems to be higher in argon than in nitrogen atmosphere.

3.3 Sintering of Ti-TiN nano-composites

Figures 2(b) to 2(c) show the variation in sintered density as a function of sintering temperature for compacts of Ti-8wt%TiN and Ti-15 wt%TiN sintered in argon and nitrogen atmospheres. The presence of denser TiN (p = 5.5

15th International Plansee Seminar, Eds. G. Kneringer, P. Rödhammer and H. Wildner, Plansee Holding AG, Reutte (2001), Vol. 4

gm/cm^3 for TiN as compared to p = 4.5 gm/cm^3 for Ti) tend to exhibit a higher sintered density.

Figure 3. shows the XRD pattern of elemental Ti sample, Ti-8wt%TiN and Ti-15wt %TiN nano-composites sintered in nitrogen atmosphere at 1000°C. The XRD shows that the nitrogen dissolution/reaction at the sintering temperature leads to precipitation/formation of not only the equilibrium TiN and Ti_2N phases but also various metastable phases. Due to the uncertainty of quantitative contribution of each of these phases to the overall increase in the density, it has not been possible to find the contribution of heat of reaction to the sintering rates of titanium nor is it possible to ascertain the exact level of densification of these samples.

Samples sintered in nitrogen atmosphere exhibited a golden yellow color and considerable weight increase. The X-ray diffraction analysis (Figure.3) indicated the weight increase of the samples sintered in nitrogen atmosphere could be attributed to the formation of various nitrides. A weight increase of the order of 13% - 17% for samples sintered at 1000°C, according to the Ti-N equilibrium diagram [14] should result in the formation of TiN and Ti_2N equilibrium phases, but XRD revealed the formation of other non-equilibrium phases like $TiN_{0.3}$ and $Ti_3N_{1.29}$ along with the equilibrium ones. These phases may have formed due to the non-equilibrium cooling from the sintering temperature.

Samples sintered in argon atmosphere showed an overall decrease in volume and considerable densification. Densities of the order of 85% could be reached at 1100°C which could be attributed to the fine particle size of the starting powders.

Table 1: Percentage change in radius values ($\Delta R/R_o$ x 100) as a function of sintering temperature for samples sintered in argon as well as in nitrogen atmosphere (negative indicates shrinkage while positive indicates expansion of the sintered samples).

Sr. no	Sample	900°C		950°C		1000°C		1050°C		1100°C	
		Ar	N_2	Ar	N_2	Ar	N_2	Ar	N_2	Ar	N_2
1.	Ti	-0.5	1.6	-1.2	1.9	-1.2	2.3	-2.3	2.7	-3.3	3.1
2.	Ti-8wt%TiN	-0.8	1.5	-2.6	1.7	-2.0	2.1	-2.8	2.8	-4.3	3.1
3.	Ti-15wt%TiN	-1.2	1.3	-2.1	1.8	-2.1	2.3	-2.9	2.4	-3.8	3.2

15th International Plansee Seminar, Eds. G. Kneringer, P. Rödhammer and H. Wildner, Plansee Holding AG, Reutte (2001), Vol. 4

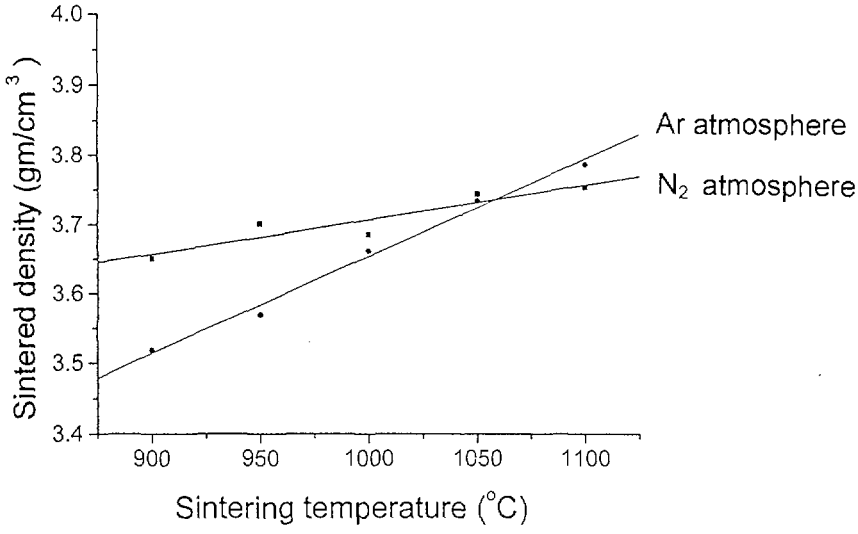

Figure 2(a): Variation of sintered density as a function of sintering temperature for pure titanium samples sintered in argon and nitrogen atmosphere.

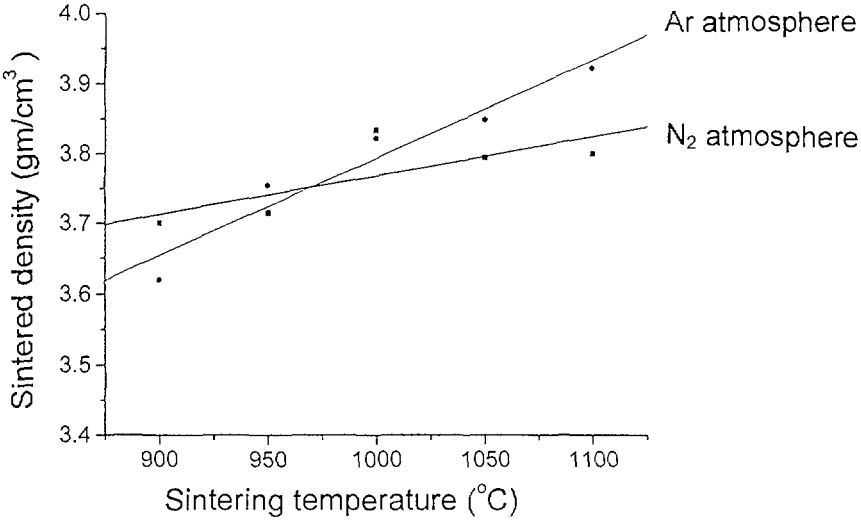

Figure 2(b): Variation of sintered density as a function of sintering temperature for Ti-8wt%TiN samples sintered in argon and nitrogen atmosphere.

15th International Plansee Seminar, Eds. G. Kneringer, P. Rödhammer and H. Wildner, Plansee Holding AG, Reutte (2001), Vol. 4

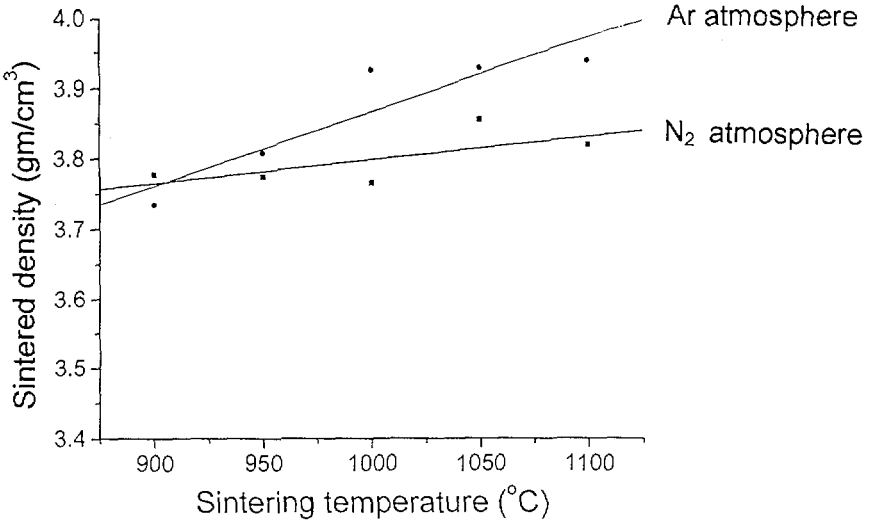

Figure 2©: Variation of sintered density as a function of sintering temperature for Ti-15wt%TiN samples sintered in argon and nitrogen atmosphere.

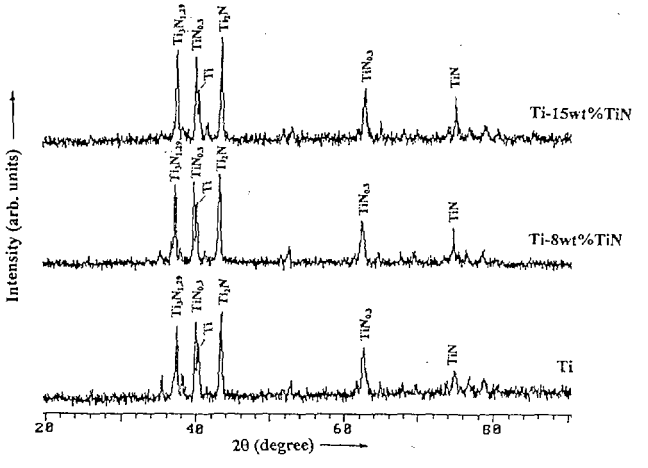

Figure 3: XRD pattern of pure Ti, Ti-8wt%TiN and Ti-15wt%TiN samples sintered at 1000°C in nitrogen atmosphere.

15th International Plansee Seminar, Eds. G. Kneringer, P. Rödhammer and H. Wildner, Plansee Holding AG, Reutte (2001), Vol. 4

Table.1 gives the percentage change in radius values as a function of sintering temperature for samples sintered in argon and nitrogen atmosphere. The shrinkage values from table.1 show a maximum shrinkage below 4% thus indicating that the sintering is confined to the initial stages of sintering.

Taking into consideration the most general expression for volume diffusion in order to study the sintering kinetics,

$$y^2 = 5.23\gamma\Omega D_v t / KTa^3 \quad \ldots\ldots\ldots\ldots\ldots\ldots \quad (1)$$

Where: $y = \Delta L/L_o \cong 1/2(\Delta R/R_o)$ = fractional radial shrinkage,
γ = surface energy (J/m^2),
Ω = volume of Ti vacancy (m^3),
D_v = volume diffusion coefficient = $D_{vo}e^{-QV/RT}$ (m^2/sec),
K = boltzmans constant,
T = temperature (^oK),
a = particle radius (m),
t = time (sec).

Since all the experiments have been performed with a rate of 1° / 2 sec, T / t = C is taken as 0.5 °K / sec. Substituting the latter, eqn. (1) can now be modified as:

$$y = (5.23\gamma\Omega / CKa^3)^{0.5}\exp -(0.5Q / RT) \quad \ldots\ldots \quad (2)$$

Figure 4(a) and 4(b) show the typical Arrhenius plots i.e. lny Vs 1/T for pure Ti samples sintered in argon and nitrogen atmospheres respectively.
The slope of the plot gives $0.5Q_D$ / KT while the intercept on the y-axis gives $0.5\ln(5.25\gamma\Omega D_o / CKa^3)$. The computed values of D_o and Q are given in table. 2 for all the specimens.

15th International Plansee Seminar, Eds. G. Kneringer, P. Rödhammer and H. Wildner, Plansee Holding AG, Reutte (2001), Vol. 4

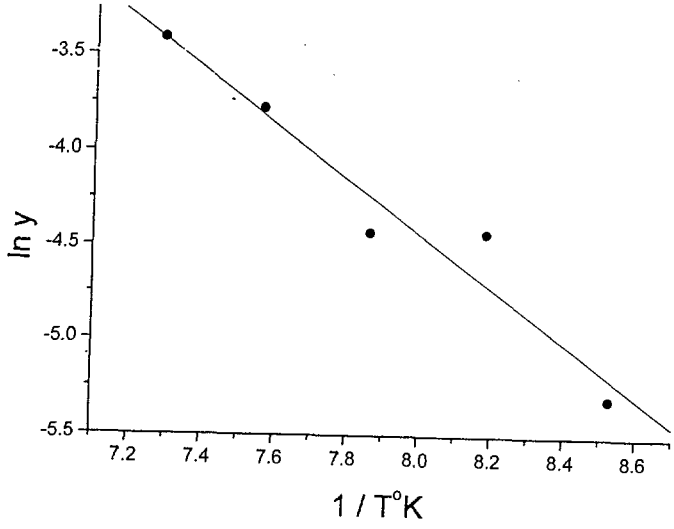

Figure 4(a): Arrhenius plot of pure Ti sintered in argon atmosphere.

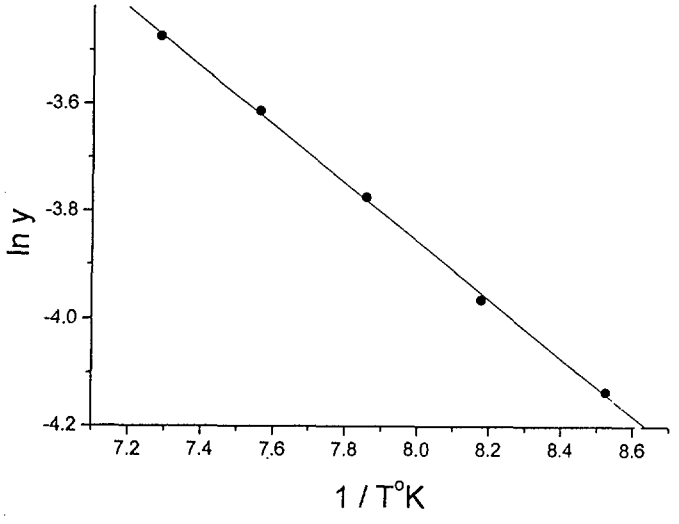

Figure 4(b): Arrhenius plot of pure Ti sintered in nitrogen atmosphere.

15th International Plansee Seminar, Eds. G. Kneringer, P. Rödhammer and H. Wildner, Plansee Holding AG, Reutte (2001), Vol. 4

Table 2: Frequency factor (D_o), activation energy (Q) and diffusion coefficients (D) for samples sintered in Ar and N_2 atmospheres.

Sr no		Ti		Ti-8wt%TiN		Ti-15wt%TiN	
		Ar	N_2	Ar	N_2	Ar	N_2
1.	D_o (m^2/s)	7.9×10^{-8}	1.7×10^{-13}	3.4×10^{-8}	6.1×10^{-13}	2.2×10^{-11}	1.2×10^{-12}
2.	Q (KJ/mol)	237.4	89.7	221.83	104	140.82	112.12
3.	D (m^2/sec)	1.3×10^{-17}	2.4×10^{-17}	3.4×10^{-17}	3.4×10^{-17}	3.1×10^{-17}	3.0×10^{-17}

Sintering of Ti in argon atmosphere required an activation energy of 237.4 KJ/mol while the D_o value obtained is $7.9 \times 10^{-8} m^2$/sec. The reported value in literature [15] of D_o varies from 1.09×10^{-2} to 4.54×10^{-6} m^2 / sec and Q values for self-diffusion of Ti vary from 131-251.2 KJ / mol. The present values obtained are in this range although both D_o and Q values are lower than the reported values.
Change in the sintering atmosphere from Ar to N_2 had decreased the sintering activation energy drastically to 89.7 KJ/mol. Similar trend was noted in Ti-8wt%TiN and Ti-15wt%TiN samples.

The lower values of activation energy in general were observed in systems where the thickness of the defective interparticle region is likely to be larger than the neck dimensions [16], in such a case it is difficult to distinguish between volume diffusion and grain boundary diffusion mechanisms as both these are taking place through a defective interparticle region and hence can be classified as boundary enhanced diffusion.

Addition of TiN to samples that are sintered in Ar in general decreased the activation energy of sintering. This could be due to the active nano sized TiN particles (may be even metastable in composition) in contact with Ti causing diffusion of nitrogen along the surfaces.

Sintering of samples in N_2 atmosphere is likely to be dominated more by the in situ nitride formation which is exothermic in nature. Almost all the samples

15th International Plansee Seminar, Eds. G. Kneringer, P. Rödhammer and H. Wildner, Plansee Holding AG, Reutte (2001), Vol. 4

have expanded during sintering possibly due to formation of several nitrides as confirmed by XRD. Thus the observed activation energy is a combination of energy required by the system for sintering and energy given out during nitridation. At this stage it is difficult to determine the separate contribution of each of these mechanisms.

Using the D_o and Q values the diffusion coefficient D at 1000°C was computed, the values of which are shown in table.2. It is evident from the table that although the D_o and Q values are varying, D remained more or less constant at 3.0 - 3.4 x 10^{-17} m^2/sec for all the systems excepting in the case of Ti sintered in pure Ar where it is 1.3 x $10^{-17}$$m^2$/sec.

The observed D values at 1000°C are smaller than those reported for self-diffusion of titanium in β-titanium [15]. Further the magnitude of D suggests that it is more likely to be related to the self diffusion of nitrogen in titanium nitrides (this is perhaps the reason that the computed D values for systems sintered both in N_2 as well as in Ar are nearly the same). During the early stages of sintering the nitrogen in the pores is likely to react with the titanium particles to form titanium nitrides. Further growth of this layer depends on the self diffusion of N_2/Ti through the layer either way. Over a period of time sufficient amounts of nitrides will be formed. The lower value of activation energy were observed in systems where the thickness of the defective interparticle region is likely to be larger than the neck dimension (as mentioned earlier). In the present case the micron sized titanium particles are associated with a large free surface which is likely to contain adsorbed species such as O_2 and N_2 from the atmosphere and also surface defects. When such particles are brought into contact, the defective region at the point of contact is much larger in thickness than the interparticle neck width. In such a case the large sized nitrogen ion diffuses through the grain boundary to the neck surface while the smaller titanium ion is transported to the neck surface by lattice diffusion. However, since the neck width is much smaller than the width of the interparticle defective region both the diffusion processes take place through this defective region. In fact this process can now be called boundary enhanced diffusion [16].

The lack in variation in D values suggests that the contribution of diffusion process towards sintering of Ti-TiN mixtures and Ti in nitrogen atmosphere is minimal as compared to formation of titanium nitride by chemical reaction. Since the latter is an exothermic reaction the decrease in observed activation energies can also be justified by the same reason.

15th International Plansee Seminar, Eds. G. Kneringer, P. Rödhammer and H. Wildner, Plansee Holding AG, Reutte (2001), Vol. 4

Figures 5(a) to 5(c) shows the SEM micrographs of the Ti sample, Ti-8 wt%TiN and Ti-15wt% TiN nano-composites sintered in argon atmosphere at 1000°C while figures 5(d) to 5(f) show the SEM micrographs of the Ti sample, Ti-8wt%TiN and Ti-15wt%TiN nano-composites sintered in nitrogen atmosphere at 1000°C. The SEM micrographs of samples sintered in N_2 and Ar atmospheres reveal distinct features. The Ar sintered samples show increasingly well dispersed TiN particles among the micron sized Ti particles. Since the sintering process is in the initial stages considerable amount of porosity can be seen. The N_2 sintered samples on the other hand showed the entire sample surface to be covered by TiN filling where this film has got ruptured the inside structure is seen consisting of coarse TiN particles and porosity.

4. CONCLUSION:

1. Initial stage of sintering of pure Ti as well as of Ti-TiN nano-composites has been studied by using constant rate of heating technique. The frequency factor evaluated varied between 7.9×10^{-8} to $2.2 \times 10^{-11} m^2/s$ in Ar atmosphere and between 1.7×10^{-13} to 1.2×10^{-12} m^2/s in N_2 atmosphere. The values are in the same range as those reported in literature.
2. The activation energy for sintering of Ti specimens in N_2 atmosphere is somewhat lower than the reported values and varied between 89.7 - 112.12 KJ / mol. It is believed that this is most likely due to grain boundary enhanced diffusion predominating in such fine particulate system.
3. Sintering of Ti and Ti-TiN nanocomposite samples in N_2 atmosphere is affected by two competing mechanisms such as endothermic energy requirement for mass transport and an exothermic in situ nitridation reaction. More work is required to evaluate the individual contribution for each of these mechanisms.
4. The lack of variation in the D values suggest that the sintering of Ti in nitrogen atmosphere and Ti-TiN nanocomposites in argon atmopshere as well as in nitrogen atmosphere is most likely controlled by the nitridation reaction rather than by the diffusion process.

15th International Plansee Seminar, Eds. G. Kneringer, P. Rödhammer and H. Wildner, Plansee Holding AG, Reutte (2001), Vol. 4

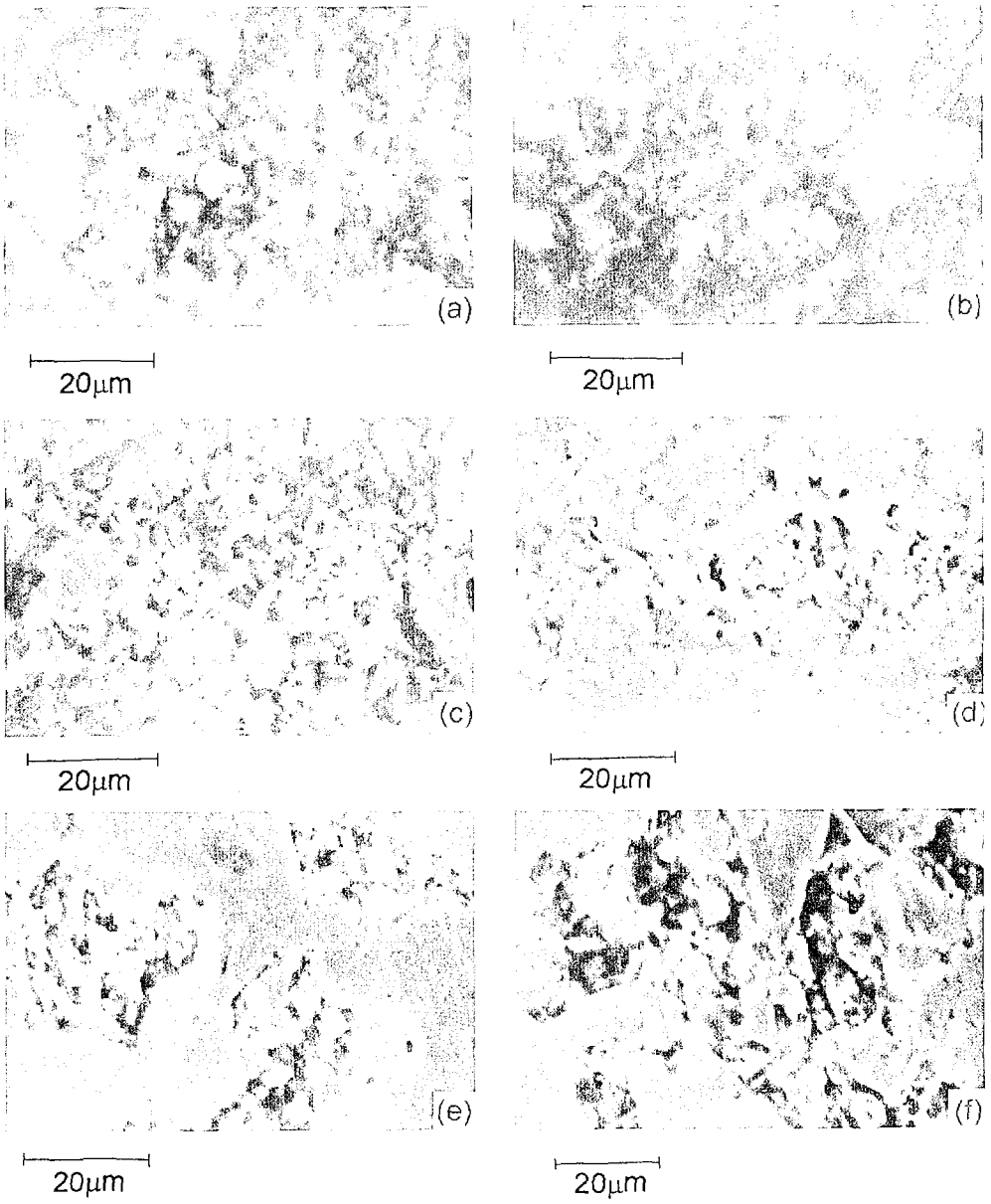

Figure 5: SEM micrograph of (a) pure Ti, (b) Ti-8wt%TiN, (c) Ti-15wt%TiN samples sintered at 1000°C in argon atmosphere and SEM micrographs of (d) pure Ti, (e) Ti-8wt%TiN, (f) Ti-15wt%TiN samples sintered at 1000°C in nitrogen atmosphere.

15th International Plansee Seminar, Eds. G. Kneringer, P. Rödhammer and H. Wildner, Plansee Holding AG, Reutte (2001), Vol. 4

REFERENCES:

1. K.H. Kramer, "Titanium applications - a critical review", Proceedings of The Sixth World Conference on titanium 1988, Part 1, Edited by P. Lacombe, B.Trieot, G.Beronger, pp.523-529.
2. T.R. Rama Mohan, T.S. Murty, P. Ramakrishnan and Elazer Y. Gutmanas,"Titanium nano-composite powders by attribution milling", Advances in Powder Metallurgy and particulate Materials, APMI, Compiled by Charles L. Rose and Martin H. Thibadeau, Metal Powder Industries Federation, Vol. 1, 1999, pp. 159-164.
3. Peter C. Eloff, Sintering of titanium, Metals Handbook (Ninth Edition), Vol. 7, Powder Metallurgy, ASM Handbook Committee, Coordinator Erhard Klar, 1984, pp. 393-399.
4. V.S. Arunachalam, "Powder Metallurgy of Titanium", Titanium and Alloys, vol. 3, The Metallurgical Society of AIME Proceedings, Edited by J.C. Williams and A.F. Below, pp. 2305-2314.
5. V.S. Ustinov, A.M. Petrunka, Yu G. Olesov and R.K. Ogner, "A novelty in The field of titanium powder metallurgy", Titanium and Titanium Alloys, Vol.3, The Metallurgical Society of AIME Proceedings, Edited by J.C. Williams and A.F. Belov, pp.2315-2321.
6. S. Ranganath, "A review on particulate reinforced titanium matrix composites", *Journal of Materials Science*, 32, 1977, pp. 1-16.
7. Shierif M. El-Eskandarany, Omari, M., Konno T.J., Sumiyama K., Hirai T. and Suzuki, K., "Synthesis of full-density nanocrystalline titanium nitride compacts by plasma-activated sintering of mechanically reacted powder", *Metallurgical and Materials Transactions A,* Vol. 29A, July 1998, pp.1973-1981.
8. P.S. Goodwin, A. Wisbey, H.S. Ubhi, Z. Kulikowski, P. Gasson, and C.M. Wardclose, "Synthesis of particulate reinforced titanium MMC by Mechanical alloying", Titanium 95: Science and Technology, Vol. III, Proceedings of the Eight World Conference on titanium, Edited by P.A. Blenkinsop, W.J. Evans, H.M. Flower, pp. 2874-2881.
9. C. Suryanarayana, "Nanocrystalline Materials", *International Materials Reviews, 1995*, Vol. 40, pp.41-115.
10. V.V Dabhade, M.M Godkhindi, T.R. Rama Mohan and P. Ramakrishnan, "Nitridation reaction during sintering of mechanically milled titanium powders," communicated.
11. B. Gunther and A. Kumpmann, "Ultrafine oxide powders prepared by Inert gas evaporation", *Nanostructured Materials*, Vol. 1, 1992, pp. 27-30.

15th International Plansee Seminar, Eds. G. Kneringer, P. Rödhammer and H. Wildner, Plansee Holding AG, Reutte (2001), Vol. 4

12. S. Amarchand, T.R. Rama Mohan and P. Ramakrishnan, " A novel chemical solution technique for the preparation of nano size titanium powders from titanium dioxide," Advanced Powder Technology," Vol.2, No.4, (2000), pp. 415-422.
13. M.J. Mayo,"Processing of nanocrystalline ceramics from ultrafine particles," *International Materials Reviews*, 1996,Vol.41,No.3, pp.85-113.
14. "ASM Engineered Materials Reference Book," Reference publications, ASM INTERNATIONAL, (1989), Materials Park, Ohio, USA, p.257.
15. R. Sundaresan, A.C. Raghuram, R.M. Mally and K.I. Vasu," Sintering of β Titanium: role of dislocation pipe diffusion," *Powder Metallurgy*, 1996,Vol 39, No.2, pp. 138-142.
16. D.L Johnson and L. Berrin, "Grain boundary diffusion in the sintering of oxides," Sintering and related phenomena, Ed. G.C.Kucznsk, N.A. Hooton and C.F.Cubbor, Gordon and Breach, New York, 1967.

15th International Plansee Seminar, Eds. G. Kneringer, P. Rödhammer and H. Wildner, Plansee Holding AG, Reutte (2001), Vol. 4

Title: **SINTERING OF NANODIAMOND IN THERMODYNAMIC STABILITY AREA OF DIAMONDS**

Authors: A.V. Nojkina[1], N.A. Kolchemanov[1], P.Ya. Dedkov[2]

Affiliation: [1] VNIIALMAZ, Moskow, Russia;
[2] VNIITF, Snezhinsk, Russia

Diamond powders UDA have mentioned below physico-chemical propeerties:

- light-grey colour
- grain size 0,02-0,004 mkm (biggest grain size is 20nm, smallest - 4nm), it is permitted the presence of the lumps. It is found the separate microcrystals with size 60-90nm.
- density - 2.97 - 3.0 g/cub.sm.
- specific surface - 250-350 sq.m/g.
- moisture - 3.00% mass.
- admixtures (incombustible residue) - less than 2.0% mass.
- admixture mass, less then: iron - 0.025% mass., manganese - 0.01% mass., molybdenum - 0.01% mass., lead - 0.04% mass., sulphur - 0.38% mass., chlorine - 0.33% mass.
- temperature of beginning of intensive gas emission under heating in air - 753K
- crystal structure of the UDA - cubic and hexagon (hexagular)
- element composition of UDA: carbon - 86.91% mass., nitrogen - 1.92% mass., hydrogen -0.78% mass., oxygen - 9.2% mass., organic and inorganic functional groups, water.

15th International Plansee Seminar, Eds. G. Kneringer, P. Rödhammer and H. Wildner, Plansee Holding AG, Reutte (2001), Vol. 4

According results of emissive spectrum analysis the admixtures content does not exceed 2%. Ni and Mn are the active catalyst of grafitization, but their content is two degrees lower then in the diamonds of stationary synthesis.

Specific surface of nanodiamond powders is ten times more than shecific surface of diamond micropowders of stationary synthesis. That's why it is possible to consider that UDA contains the less quantity of the admixtures than the diamonds of stationary synthesis.

It was studied the surfaces of ten types of diamond powders of dynamic synthesis and natural diamond powders. Method of the thermoprogrammed desorption and mass-spectrometric analysis of desorption products were used for this study of the surfaces. Fig. 1-4 show the kinetic curves of H_2O and CO_2 desorption. It was found that the composition and the state of the surface of the powders UDA and BDA differ essentially. The mass-spectrums corresponding to temperature 400°C witness this. It was found that mainly the water and carbon dioxid are on the surface of UDA powders, but besides of the water and carbon dioxid the hydrocarbons with M=58 a.w. are on the surface of BDA powders.

It has been studied kinetics of desorption of H_2O and CO_2 under linear heating of the powders to 400°C. The characteristic curves of H_2O and CO_2 desorption are shown at fig.1. It may be seen that the surfaces of studied types of powders have the strong sorption activity to H_2O. Desorption curves pass through two or three maximums of desorption rate. It depends on the types of powders and witnesses of presence of few active adsorption centers on the surface. Physically adsorbed water has poor bond with the surface and is moved away under low temperature.

We have studied the surfaces of natural diamond powders too. The characteristic features of the last ones are the biggest content of CO with ac-

15th International Plansee Seminar, Eds. G. Kneringer, P. Rödhammer and H. Wildner, Plansee Holding AG, Reutte (2001), Vol. 4

tivation energy of 7.9 kJ/mol and nearly absolute lack of CO_2 sorption on the surface.

Superhard materials of different sorts of detonation diamond powders have been made at the press-device DO-137A in the high-pressure chamber "toroid" - type. The same eqwipment was used for making of the composite diamond-content materials ofLDA and UDA mixes with static synthesis diamonds and impregnating material.

Sinters density rises with increase of pressure. This fact was established in the course of sintering of the different marks of acto nation diamond powders.

The maximum density that was obtained under the pressure of 90 kbar in the AVD "toroid" - type is different for tested marks. It is: for BDA - 24 g/sq. sm.; LDA - 2.4 g/sq. sm.; UDA - 2.35 g/sq. sm.

Density of the sinters that were obtained in polypuncheon apparatus under the pressure 80 kbar over 18 hours is 3.1 for LDA and 2.9 for BDA. It is higher than density of the sinters that were obtained in AVD"toroid" - type, but it is somewhat lower than density of the sinters natural submicron powders.

Density decreases in the row: LDA-BDA-UDA. It corresponds with density volume of the tested powders (, , 3,23; 3,0; 2,9) g/cub. sm. and corresponds with available data of OES. It was determined that density rises with increase of the lonsdeylite content. So rise of the sample density depends of pressure and percentage content of the lonsdeylite. It was explained not only by the porosity decrease with the pressure rise but by increase of the share of diamond bonds in the sample. It corresponds with available data of OES (fig. 5) and with results of ratio-phase analysis of the sinters.

It was studied the carbon states in the experimental samples (fig.5). Quantitative measuring has shown that carbon state, corresponding to SP^3 -

15th International Plansee Seminar, Eds. G. Kneringer, P. Rödhammer and H. Wildner, Plansee Holding AG, Reutte (2001), Vol. 4

hybridization, is less expressed for the samples of UDA type than for the samples of LDA type.

Influence of the pressure on transformation of the graphite to diamond was studied too. It was found out that the pressure increase from 75 to 115 atm leads to displacement of CIS maximum the direction of the maximum in the natural diamond spectrum (fig.6). We think that this fact is conditioned by increase of the portion of carbon that has turned into diamond. Displacement of CIS maximum for sinter of the powder UDA (P_1=75 atm; U=3,5 V) is 0,8 mV and for the same sinter under P=115 atm and U=3,5 V the displacement is 0,5 mV.

It was studied the temperature influence on the sinters properties. It was determined that the density rises with the temperature increase under sintering in the area of the diamond stability. Density decrease under the temperature corresponding to the area of the diamond metastability (fig.7). The impregnation increases the density to a greater degree than the mixture sintering (up to 3.2 g/cub. sm.), and temperature does not influence on the density . . It witness about high thermal stability of the samples. Density of the sinters, that were obtained of the original diamond powders of detonation synthesis, decreases at the temperature higher than 1800°C. But density of the sinters, that were obtained of diamond powders of detonation synthesis with silicon impregnation does not decrease up to the temperature 2400°C.

Thus, it was determined that PCD samples of LDA with the density more than 3.2 g/cub. sm. may be obtained by means of impregnation with liquid metals in Russian apparatus AVD "toroid" - type. Made PCD are characterized by thermal stability more than 1200°C. Their hardness is more than 6000kg/mm^2, cracking resistivity - 10 MPa/m^{0,5}.

15th International Plansee Seminar, Eds. G. Kneringer, P. Rödhammer and H. Wildner, Plansee Holding AG, Reutte (2001), Vol. 4

Experimental sintering of LDA, UDA, BDA has determined the correlation between quality of the sinter and quality of original diamonds of detonation synthesis.

The same correlation has been obtained for diamonds of statical synthetics in comparison with natural diamonds. In shot, the more perfect is the structure of original raw materials, the higher are the physico-mechanical properties of obtained sinters.

The strength of diamond powder of 60/70 mesh obtained from crushed sinter samples was measured to estimate the quality of the diamonds. After the test was complated it was found that the strength of the powders obtained from the nanodiamond sinters corresponds with the strength of the analogous fraction of the polycrystalline powders obtained from the diamonds made under static synthesis conditions.

In the conclusion we consider sintering of nanodiamonds as the good option to use them in the wearproof tools and composites

15th International Plansee Seminar, Eds. G. Kneringer, P. Rödhammer and H. Wildner, Plansee Holding AG, Reutte (2001), Vol. 4

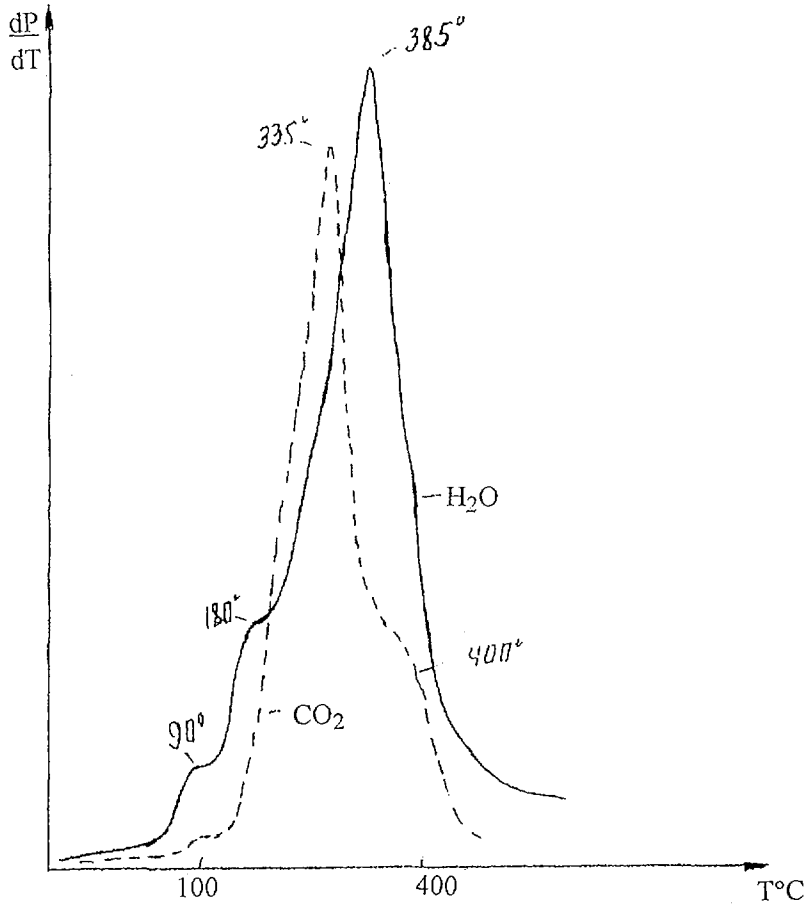

Fig.1 Kinetic of H_2O and CO_2 desoprtion from the surface of power UDA.

15th International Plansee Seminar, Eds. G. Kneringer, P. Rödhammer and H. Wildner, Plansee Holding AG, Reutte (2001), Vol. 4

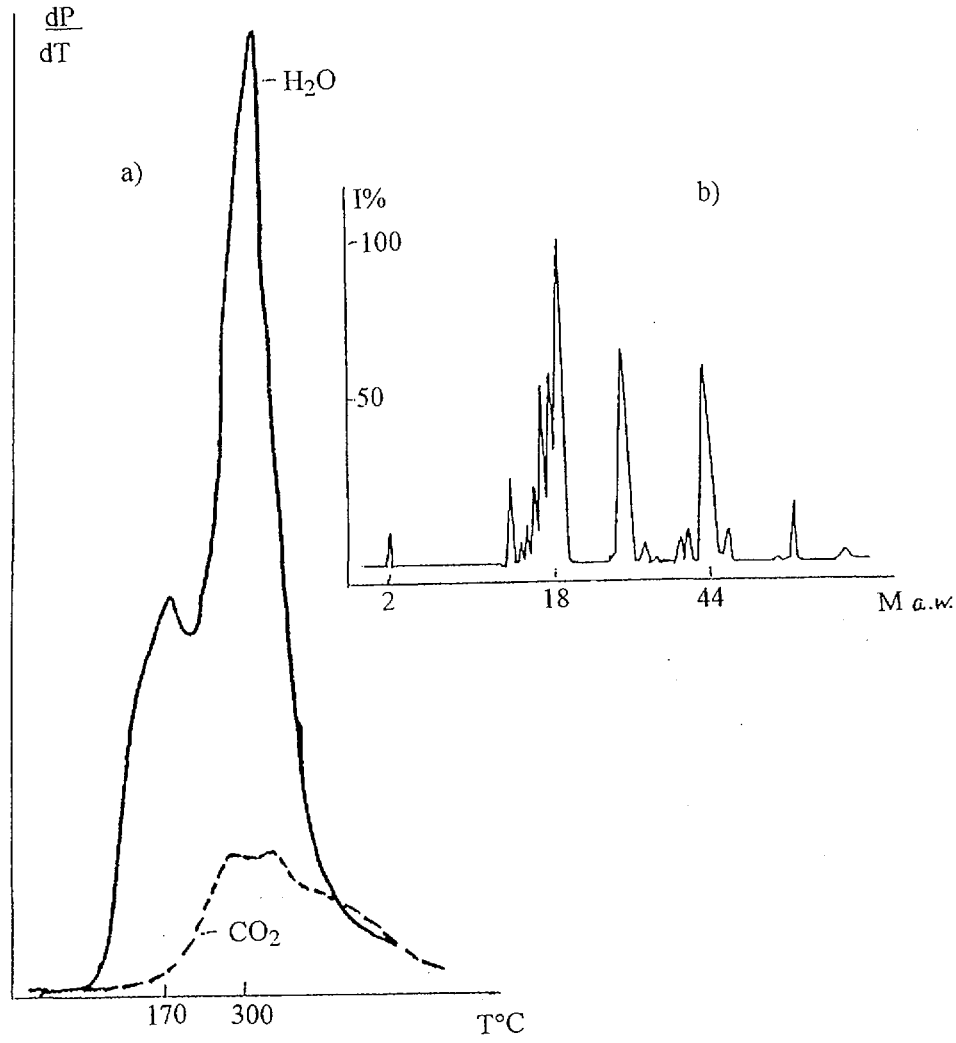

Fig. 2 Kinetic of H_2O and CO_2 desorption from the surface of the UDA (a) и and mass – spectrograms of destruction under 400°C (b).

15th International Plansee Seminar, Eds. G. Kneringer, P. Rödhammer and H. Wildner, Plansee Holding AG, Reutte (2001), Vol. 4

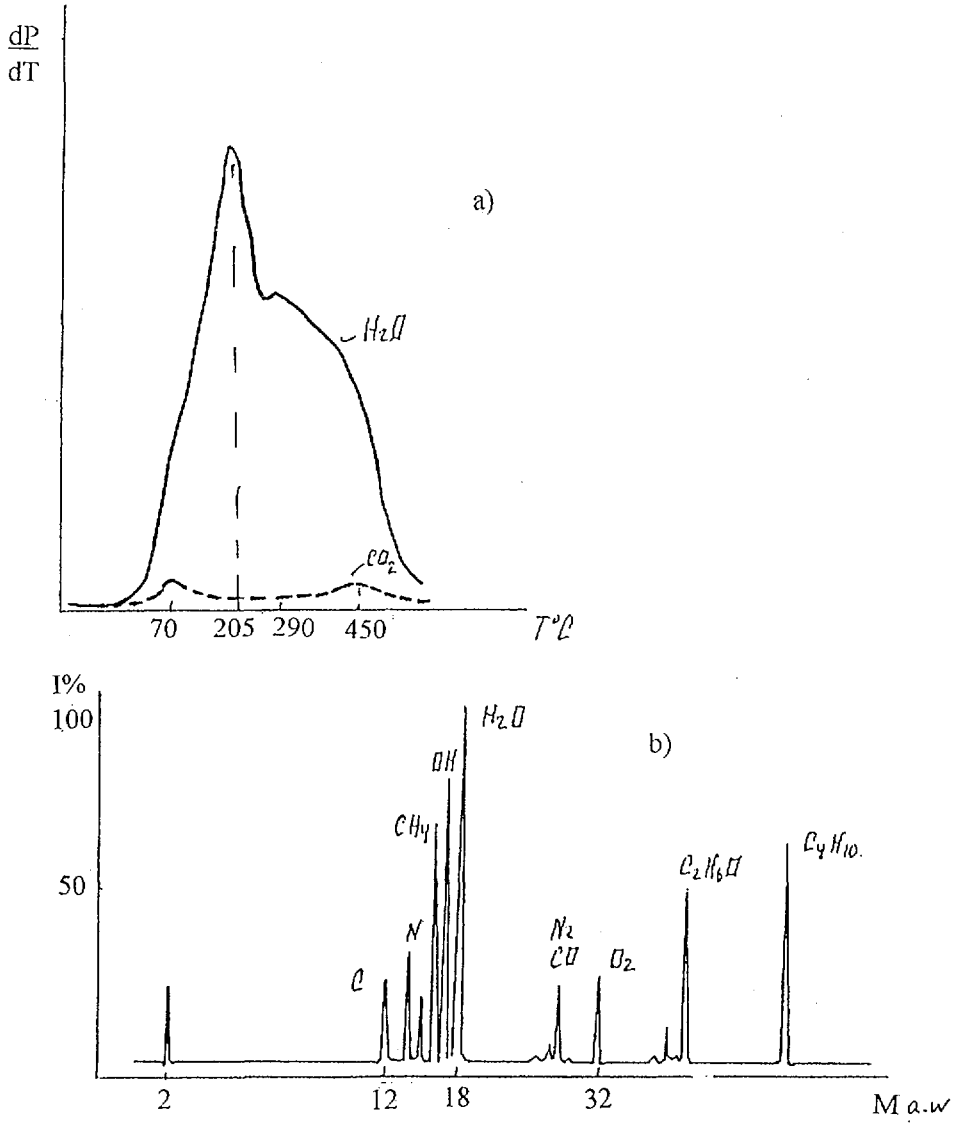

Fig. 3 Kinetic of H_2O and CO_2 desorption from the surface of the BDA (a) and mass – spectrograms of destruction under 400°C (b).

15th International Plansee Seminar, Eds. G. Kneringer, P. Rödhammer and H. Wildner, Plansee Holding AG, Reutte (2001), Vol. 4

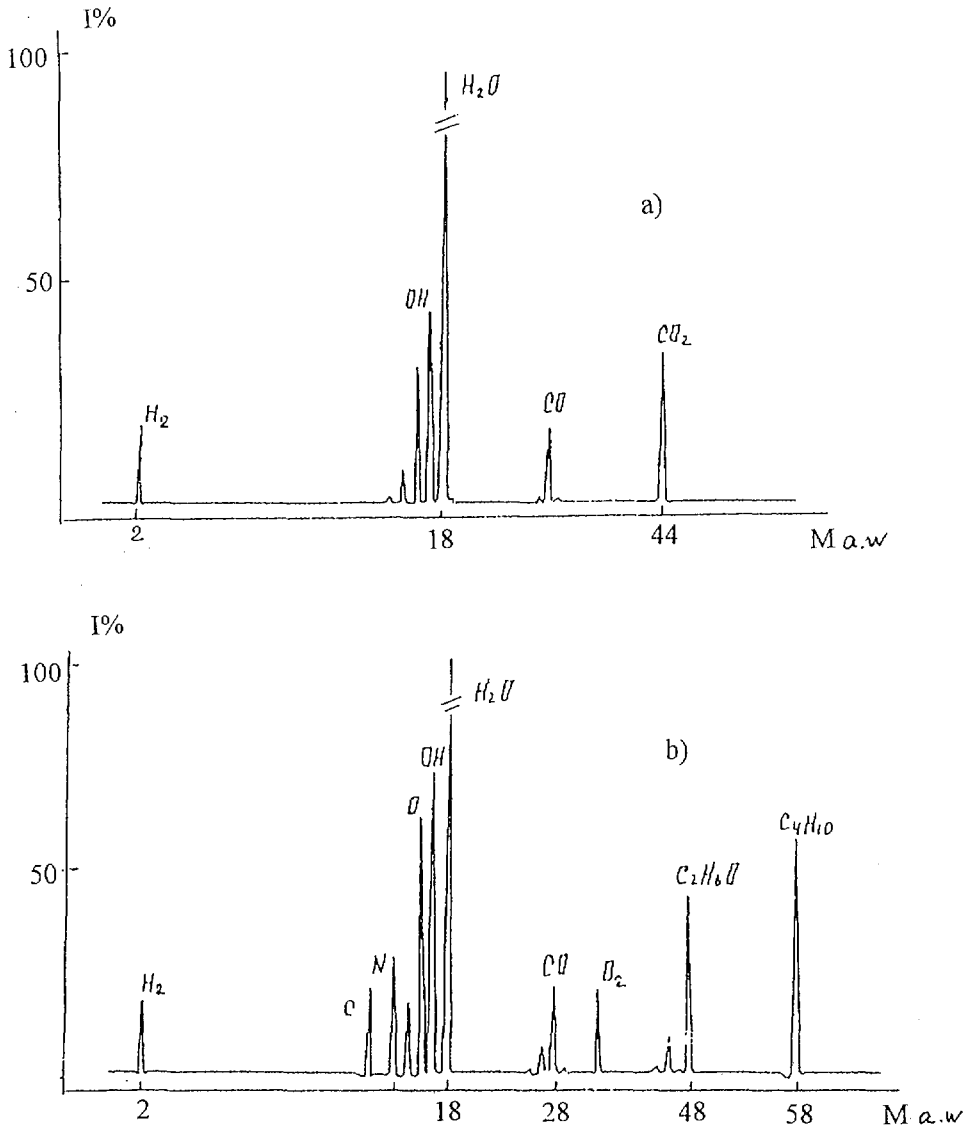

Fig.4 Mass – spectrums of the powders UDA and BDA desorption. Heating temperature 400°C.

15th International Plansee Seminar, Eds. G. Kneringer, P. Rödhammer and H. Wildner, Plansee Holding AG, Reutte (2001), Vol. 4

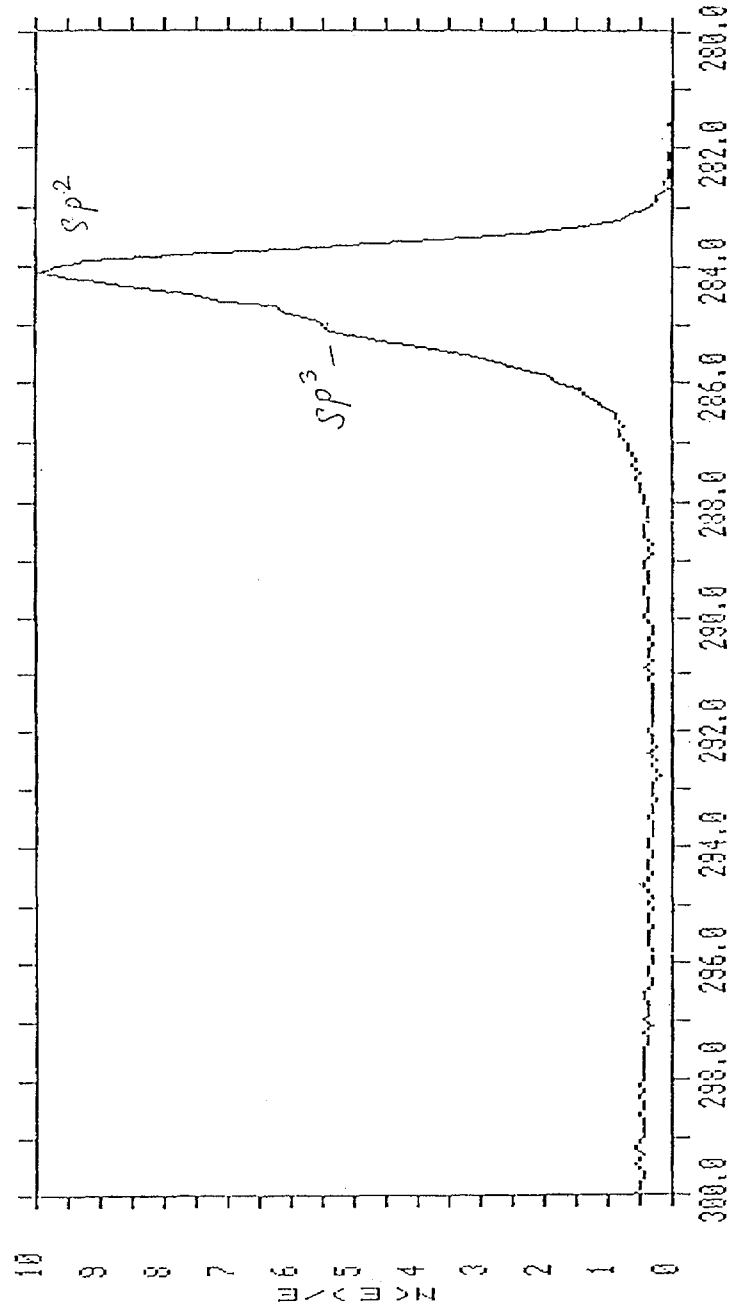

Fig.5 Carbon line of the C/S natural diamond surface of LDA sample (P=95 atm, U=3.5V).

15th International Plansee Seminar, Eds. G. Kneringer, P. Rödhammer and H. Wildner, Plansee Holding AG, Reutte (2001), Vol. 4

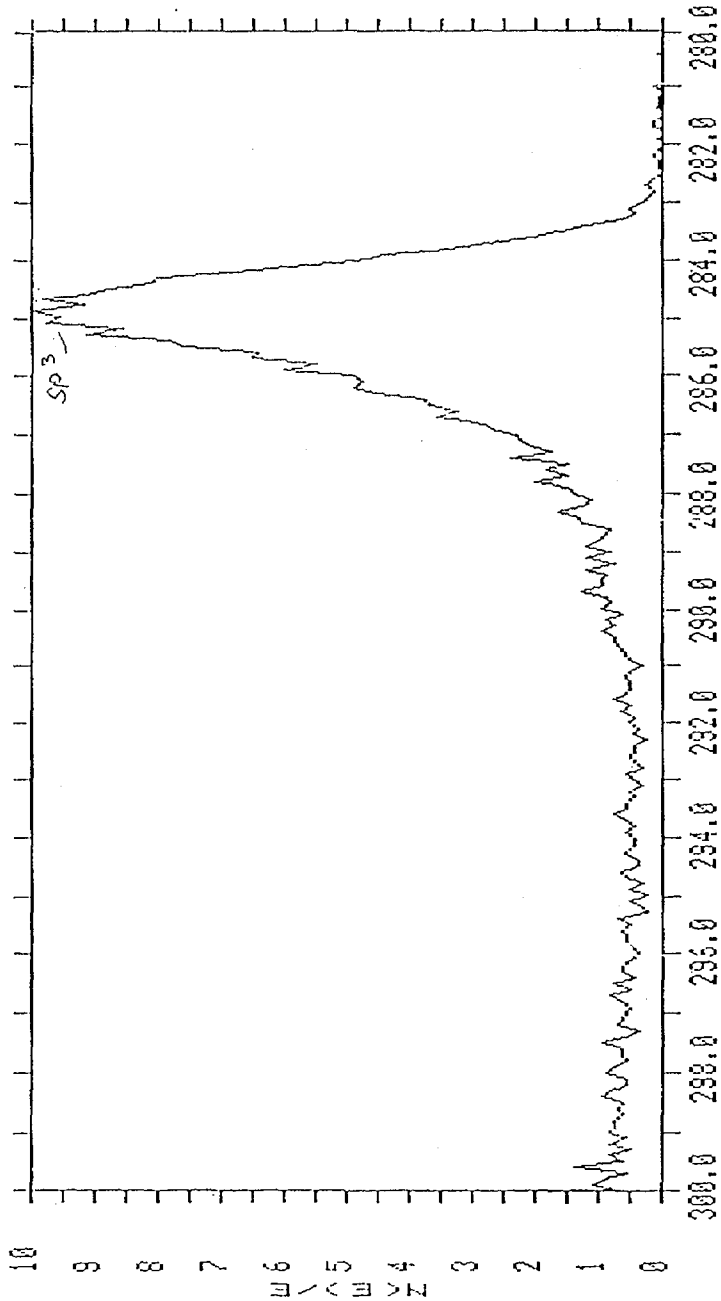

Fig. 6 Carbon line of the C/S natural diamond surface.

15th International Plansee Seminar, Eds. G. Kneringer, P. Rödhammer and H. Wildner, Plansee Holding AG, Reutte (2001), Vol. 4

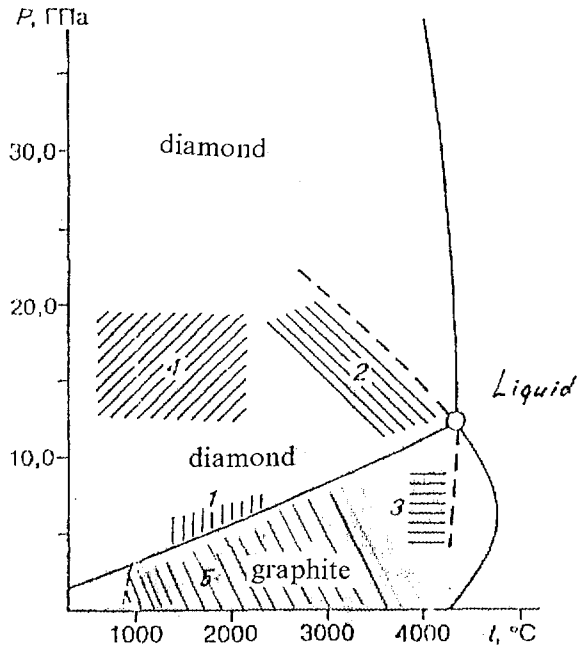

Fig 7 Phase diagram for element carbon (Bandy, 1989)

1 – area of the catalytic in metal presence diamond synthesis of graphite;

2 – area of direct transformation between graphite and diamond;

3 – area of direct transformation between diamond and graphite;

4 – area of direct transformation between graphite and lonsdaylit;

5 – area of the catalytic transformation between diamond and graphite.